PLOS COMPUTATIONAL BIOLOGY

RESEARCH ARTICLE

Spatial kinetics and immune control of murine cytomegalovirus infection in the salivary glands

Catherine M Byrne[1], Ana Citlali Márquez[2], Bing Cai[3], Daniel Coombs[4], Soren Gantt[5]*

1 Vaccine and Infectious Disease Division, Fred Hutchinson Cancer Center, Seattle, Washington, United States of America, **2** British Columbia Centre for Disease Control, Vancouver, British Columbia, Canada, **3** British Columbia Children's Hospital Research Institute, Vancouver, British Columbia, Canada, **4** Department of Mathematics, The University of British Columbia, Vancouver, British Columbia, Canada, **5** Département de Microbiologie, Infectiologie et Immunologie, Université de Montréal, Montréal, Québec, Canada

* soren.gantt@umontreal.ca

OPEN ACCESS

Citation: Byrne CM, Márquez AC, Cai B, Coombs D, Gantt S (2024) Spatial kinetics and immune control of murine cytomegalovirus infection in the salivary glands. PLoS Comput Biol 20(8): e1011940. https://doi.org/10.1371/journal.pcbi.1011940

Editor: Rustom Antia, Emory University, UNITED STATES OF AMERICA

Received: February 22, 2024

Accepted: July 30, 2024

Published: August 16, 2024

Data Availability Statement: All data and code used for running experiments, model fitting, and plotting is available on a GitHub repository at https://github.com/catherinebyrne/MCMV-primary-infection.

Funding: This work was supported by a grant from the Natural Sciences and Engineering Council of Canada to SG, number RGPIN-2018-05666. The funders did not play any role in the study design, data collection and analysis, decision to publish, or preparation of the manuscript.

Abstract

Human cytomegalovirus (HCMV) is the most common congenital infection. Several HCMV vaccines are in development, but none have yet been approved. An understanding of the kinetics of CMV replication and transmission may inform the rational design of vaccines to prevent this infection. The salivary glands (SG) are an important site of sustained CMV replication following primary infection and during viral reactivation from latency. As such, the strength of the immune response in the SG likely influences viral dissemination within and between hosts. To study the relationship between the immune response and viral replication in the SG, and viral dissemination from the SG to other tissues, mice were infected with low doses of murine CMV (MCMV). Following intra-SG inoculation, we characterized the viral and immunological dynamics in the SG, blood, and spleen, and identified organ-specific immune correlates of protection. Using these data, we constructed compartmental mathematical models of MCMV infection. Model fitting to data and analysis indicate the importance of cellular immune responses in different organs and point to a threshold of infection within the SG necessary for the establishment and spread of infection.

Author summary

Cytomegalovirus (CMV) is the most common congenital infection and causes an enormous burden of childhood disease. To gain insight into the immune requirements for controlling infection, we used a mouse model to reproduce characteristics of natural CMV infection, employing a low viral inoculum, and delivering the virus to the salivary glands (SG), a key site of CMV replication. Our results provide detailed data on the spatial and temporal spread of infection throughout the body and identify key immune correlates of the control of viral replication. By translating these findings into mechanistic mathematical models, we revealed the importance of organ-specific immune responses, particularly the requirement of TNF-α and IFN-γ to control infection within the salivary glands.

Competing interests: SG received consulting fees from Moderna, Merck, GSK, Seqirus and Curevo, and research support from Moderna, Merck, GSK, Pfizer, and Altona Diagnostics.

Furthermore, our mathematical modeling allowed us to compare known characteristics of human CMV infection related to infection establishment and spread to those predicted in mice, underscoring the suitability of the MCMV model to study its human homologue. These insights provide guidance for developing targeted vaccines to prevent CMV infection and disease.

Introduction

Human cytomegalovirus (HCMV) is a β herpesvirus that infects the majority of the world's population [1]. HCMV establishes life-long infection, primarily acquired via mucosal exposure to virus shed in body fluids, such as saliva, urine, and breast milk, of infected individuals [2,3]. HCMV is also the most common congenital infection, occurring in roughly 0.5% of all live births in high income countries, and even more frequently in low and middle-income countries [4]. A major driver of congenital infection is transmission from young children, who persistently shed virus at high levels after acquiring HCMV infection, to pregnant women [5,6]. While a tremendous amount of research has been dedicated to HCMV vaccine development, clinical trials of candidates performed to date have demonstrated, at most, around 50% protection against HCMV acquisition and have not been approved for use [7–11]. However, a recent study by our group indicates that even modestly protective vaccines may be highly effective at decreasing congenital infection if given to young children, due to their ability to reduce viral shedding and transmission to pregnant women [12]. As such, a better understanding of the determinants of the intensity and duration of viral shedding would be valuable to inform the development of vaccines to prevent HCMV transmission.

The murine (M)CMV model facilitates studies of these viral dynamics and immune control [13–20]. MCMV and HCMV genomes share a high degree of sequence homology and MCMV infection recapitulates many features of its human counterpart [21,22]. However, most MCMV experiments have involved inoculating mice with high doses of virus via the intraperitoneal (IP) or intravenous (IV) route of administration (ROA) to ensure infection, rather than simulating the typical conditions of a natural CMV infection involving mucosal exposures to lower quantities of virus [13,14,23].

HCMV infection is most often acquired orally, and viral replication in the salivary glands (SG) is detected early in HCMV infection [24]. Thus, low-dose MCMV inoculation of the SG may have particular relevance for natural HCMV exposure. HCMV shedding in saliva tends to occur at higher levels and is more prolonged than in other anatomic sites during primary infection and reactivation from latency [25–27]. In mice, the SG also appear to represent a distinct compartment of infection in which active MCMV replication lasts weeks longer than in other tissues [13,28,29]. Studies have shown that MCMV effectively prevents major histocompatibility (MHC) class I expression on infected SG cells, thus abrogating recognition and destruction by CD8 T cells, which helps to explain persistent, high-level viral shedding in saliva [30]. Rather, CD4 T cells eventually control infection in the SG through the production of the cytokines interferon (IFN)-γ and tumour necrosis factor (TNF)-α, which inhibit viral replication [20,30–32].

Different immune responses in the SG compared to the rest of the body may also explain why MCMV inoculations to this site have been shown to disseminate less frequently to the rest of the body, compared to the IP or intranasal (IN) ROA [13,14]. Indeed, human cohort studies by our group also suggest that oral HCMV replication is often self-limiting, and dies out before systemic dissemination and establishment of latent infection can occur, leading to a low

within-host reproductive number (R_0) [24,33]. Neither the within-host R_0 of MCMV nor the determinants of viral persistence in, or spread from, the SG have been defined.

To address the requirements for establishing infection, immune control at different anatomic sites, and spread from the SG, we performed low-dose MCMV intra-(I)SG infection experiments, collecting high-resolution spatial and temporal data on viral spread and immune response. With these data, we developed and tested mathematical models describing the kinetics of infection and immunity in anatomic compartments. Using these mathematical models, we also calculated the R_0 of MCMV in the SG and predicted the probability of sustained viral replication and spread upon SG infection following different viral inoculation doses. Together, these results add to our understanding of the determinants of CMV infection and dissemination.

Results

Viral loads expand faster and decay slower in the SG than in other organs

The spread of MCMV using daily live luminescence bioimaging of mice following infection with a low dose of 10^3 plaque-forming units (PFU; see Methods for dose determination) of a luciferase-tagged K181 strain of MCMV (K181-luc) to the right submandibular SG are shown in Fig 1. Virus was first noted solely at the site of inoculation (right submandibular SG), and then spread progressively throughout the body. Using two gates, we measured the strength of the luminescent signal in the SG compared to the rest of the body over time (Fig 2). Luminescence within the SG of infected mice was detectable and significantly higher (p-value <0.0005) than the background signal in uninfected mice as soon as 1 day post-infection. In the body, luminescence was not significantly greater in infected versus uninfected mice until 2 days post-infection (p-value <0.05). Despite the gating area of the body being 4.54 times larger than the gating area of the SG, the total luminescent signal in the SG was greater than that seen in the body from days 5–21 post-infection. In both the SG and body, the signal rose quickly, peaking 7 days post-infection. Within the SG, the signal fit an exponential growth rate of 0.42/day, while the rate in the body was 0.14/day. After the peak 7 days post-infection, luminescence in the body declined markedly faster than in the SG, with fit exponential decay rates of 0.12/day and 0.03/day, respectively.

Subpopulations of CD8 T cells and NK cells, but not CD4 T cells, show significant changes throughout infection

Mononuclear cells isolated from whole blood, SG, and spleen were characterized by flow cytometry using markers to identify populations of B cells, NK cells, and CD8, CD4, and $\gamma\delta$ T cells. To identify MCMV-specific CD8 cells, we included an MHC class I tetramer presenting the immunodominant IE1 epitope [15,19,34]. We also stained for activation markers KLRG1, found on effector cells [15,35–37], and CD69, which has been associated with tissue-resident CD8 and CD4 T cells [29,37]. Additional details are provided in the Methods section. The gating strategy used to identify cell populations of interest is shown in Fig A in S1 Text.

Of the cell populations examined, IE1-specific CD8 T cells showed the most significant changes in size over time compared to those seen in uninfected mice (Fig 2A). These cells peaked in population size on days 12 and 16 post infection in the blood and spleen, respectively, while in the SG the population size plateaued on day 24 and was sustained until the end of the observation period. Large, significant changes were also observed in populations of KLRG1+ CD8 T cells, KLRG1+ NK cells, and KLRG1+ CD4 T cells in infected mice (Fig 2B–2D, significance indicated). KLRG1+ CD8 T cells peaked between 12- and 16-days post-infection, depending on the site of collection, while KLRG1+ NK cells peaked between 8- and 12-days post-infection. KLRG1+ CD4 T cells peaked 8 days post-infection in spleen, 24 days

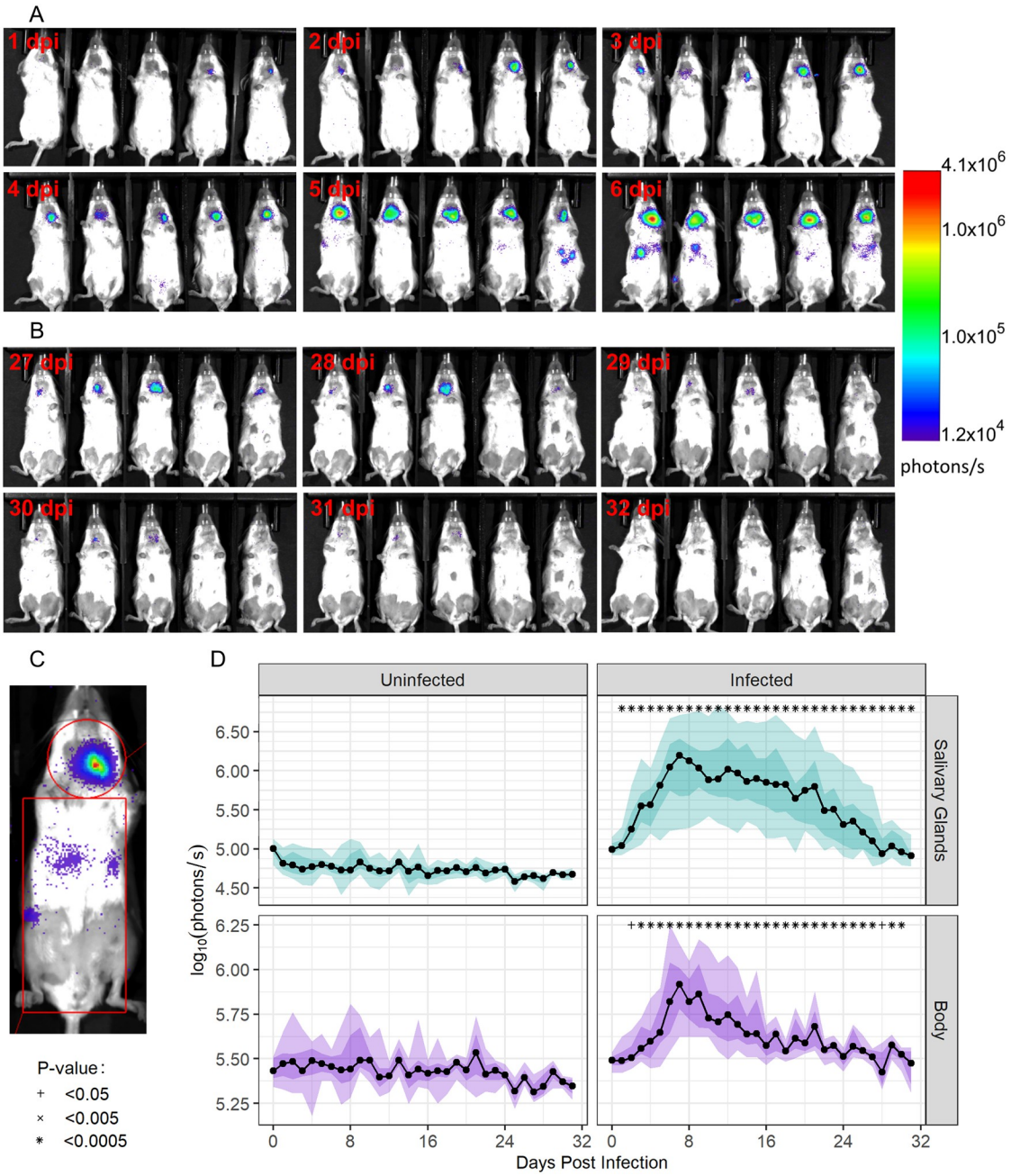

Fig 1. Spatiotemporal kinetics of viral MCMV dissemination from the SG. Bioimaging data from the first six days (**panel A**) and the last six days (**panel B**) post infection (dpi) are shown. Infection begins at the site of inoculation in the SG and disseminates throughout the body. Viral replication is greater in the SG and decays more slowly than in the rest of the body. By the end of observation (day 32), the signal within the SG has disappeared. The gates used to measure luminescent signal data in the SG separately from the other tissues (**panel C**). Longitudinal bioimaging data for these anatomical sites are shown for uninfected and infected mice (**panel D**). Symbols indicate the level of significant increase compared to background signal in uninfected mice on the same day.

https://doi.org/10.1371/journal.pcbi.1011940.g001

post-infection in the SG, and 32 days post-infection in blood. These peaks in immune cell population sizes occurred a median of four days after the peaks in viral replication, as determined by the bioimaging signals. Flow cytometry data for other immune cell populations are shown in Fig B in S1 Text. Smaller but statistically significant differences between uninfected and

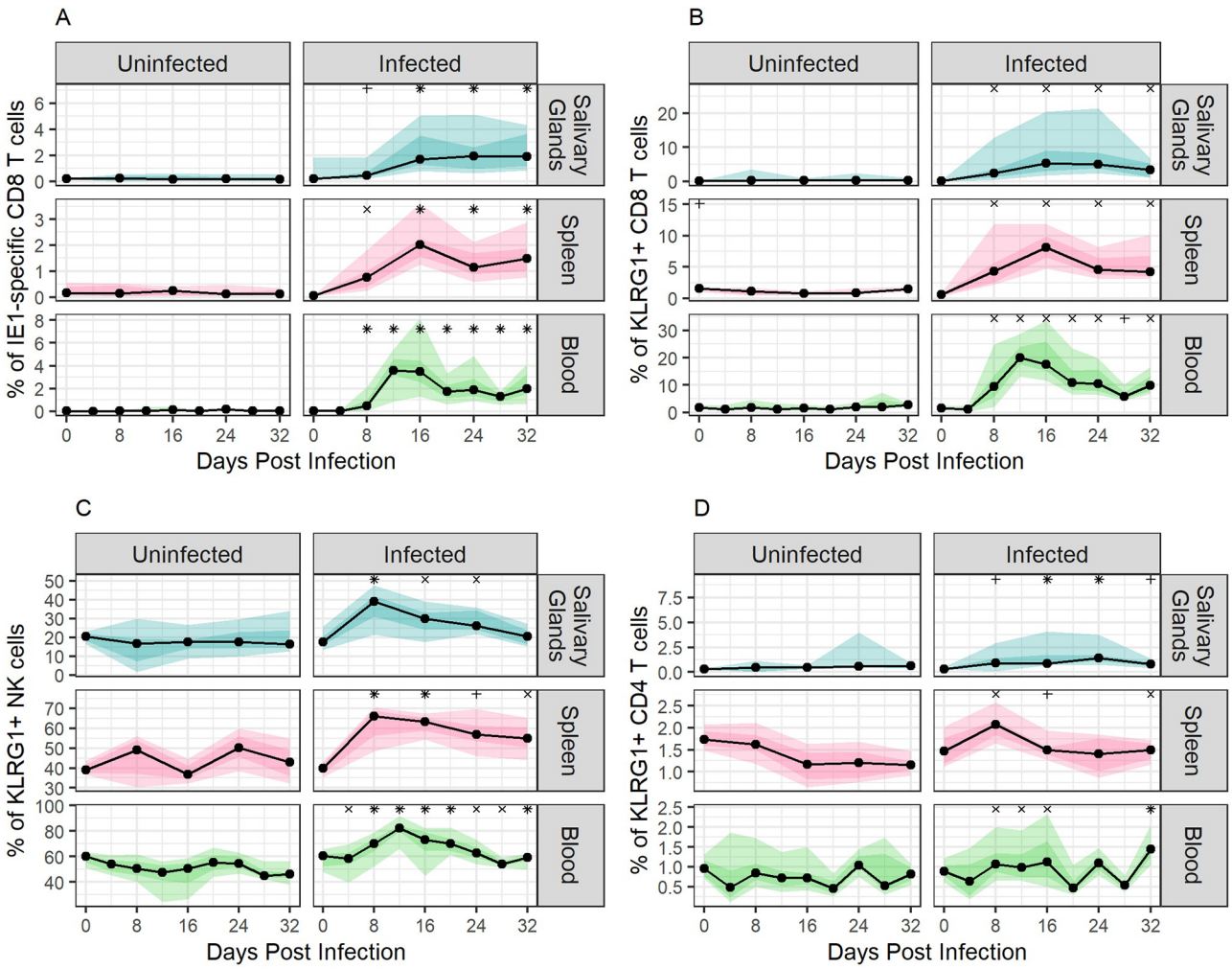

Fig 2. Expansion of immune cell populations during MCMV infection via the SG. Changes in immune cell populations within SG, spleen, and blood are shown: **panel A**, IE1-specific CD8 T cells; **panel B**, KLRG1+ CD8 T cells; **panel C**, KLRG1+ NK cells; **panel D**, KLRG1+ CD4 T cells. Immune cell population sizes are reported as the percentage of the parent population (CD8 T cells for panels A and B, NK cells for panel C, and CD4 T cells for panel D). Light ribbons show the 5–95% quantiles, dark ribbons show the 25–75% quantiles, black lines indicate median values, and dots indicate the time points at which data were collected. The symbols above the graphs indicate the level of significant increase compared to uninfected control values at the same time point, as defined in Fig 1.

https://doi.org/10.1371/journal.pcbi.1011940.g002

infected mice were noted for total populations of CD8 T cells, γδ T cells, and NK cells, consistent with previous findings that MCMV infection is primarily controlled by T cells and NK cells [15,29,38–40]. There was no discernible change in total CD4 T cells or any CD69+ cell populations over the course of infection.

We next fit exponential growth models to the immune cell population dynamics in different tissues to compare the expansion rates before the peak was reached. During early infection, the frequency of IE1-specific CD8 T cells increased most rapidly in blood (rate of 0.338/day), followed by spleen (0.228/day), and SG (0.102/day). The frequency of KLRG1+ CD8 T cells increased at similar rates in all tissues (rate of 0.238/day in the SG, 0.191/day in blood, and 0.161/day in spleen). The rates of expansion of KLRG1+ NK cells were highest in the SG at 0.099/day, followed by spleen and blood with rates of 0.063/day and 0.018/day, respectively. Despite expanding fastest in SG, KLRG1+ NK cells represented a smaller proportion of the

total NK cell population in the SG, being on average only 45.8% and 38.5% of those in the spleen and blood, respectively. The frequency of KLRG1+ CD4 T cells increased at a rate of 0.043/day in the spleen, 0.003/day in the blood, and 0.055/day in the SG.

Mathematical models of MCMV infection

Few mathematical models of the within-host kinetics of HCMV infection have been published, and even fewer of MCMV infection [15,20,41]. Based on the data we collected and information available in the literature, we created and fit two novel mathematical models to describe the dissemination of MCMV from its site of entry to the rest of the body, and to test which immune components are most important in controlling viral replication in each compartment. While NK cells are important for the control of MCMV infection, our model focuses on the role of the adaptive immune response and how it may differ within the SG compared to the rest of the body. Further, although immune measures were obtained from few anatomic sites and luminescent signals do not reliably differentiate specific visceral organs, the resolution of these data is well suited to a simplified spatial model based around ordinary differential equations, to describe the adaptive immune and viral kinetics within and between the compartments of the SG and the rest of the body.

Model 1: Infection control by IE1-specific CD8 T cells

In our base model, we assumed that the observed large expansion of IE1-specific CD8 T cells is responsible for controlling infection in both the SG and the rest of the body. We supposed that MCMV in the SG and body (V_s and V_b, respectively) infects cells (I_s and I_b, respectively) at rates η_1 and η_2, respectively. As the virus infects a wide range of different cell types but does not impair organ function in this model [22], we assumed there is no target cell limitation. These infected cells produce MCMV at a per-capita rate of p_1 and p_2 within the SG and body, respectively and naturally die at a per-capita rate, δ. Infected cells stimulate the production of IE1-specific CD8 T cells (T) at a rate $\alpha \frac{I_b+I_s}{I_b+I_s+w}$, where α is the maximum proliferation rate and w is the number of infected cells needed for the proliferation rate to reach its half-maximum. In this model, we assumed that IE1-specific CD8 T cells target and kill both I_s and I_b, following the law of mass action, with rate constant m_1 and m_2, respectively.

Upon ISG administration of MCMV, we assumed that virus is initially present exclusively in the SG. Virus from the SG and the body is assumed to disseminate to the other compartment at per-capita rates μ_1 and μ_2, respectively. Equation set (1) shows all the ordinary differential equations (ODEs) for this model and a visual representation is provided in Fig 3.

$$\begin{aligned}
\frac{dI_s}{dt} &= \eta_1 V_s - \delta I_s - m_1 I_s T \\
\frac{dV_s}{dt} &= p_1 I_s - c V_s - \mu_1 V_s + \mu_2 V_b \\
\frac{dI_b}{dt} &= \eta_2 V_b - \delta I_b - m_2 I_b T \\
\frac{dV_b}{dt} &= p_2 I_b - c V_b - \mu_2 V_b + \mu_1 V_s \\
\frac{dT}{dt} &= \alpha \frac{I_b + I_s}{I_b + I_s + w} - dT
\end{aligned} \tag{1}$$

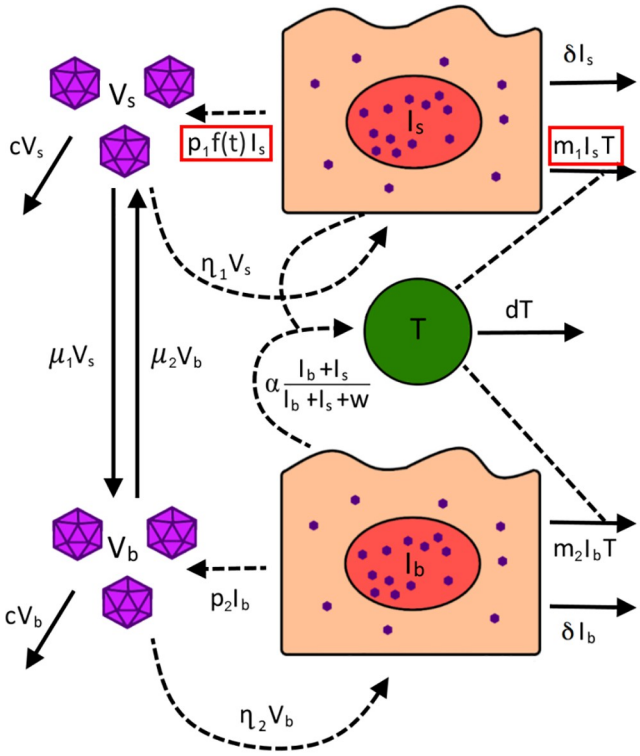

Fig 3. Visual representation of all tested models. In Model 1, infected cells in the SG (I_s) and the body (I_b) are cleared at different per-capita rates m_1 and m_2, respectively and the production rate of virus in the salivary glands is directly proportional to the number of I_s ($f(t) = 1$). In Model 2, infected cells in the SG (I_s) are assumed to no longer be cleared by CD8+ T cells ($m_1 = 0$) and the production rate of virus in the salivary glands is time dependent, where $f(t)$ is as defined as in Eq (2). Red boxes highlight the terms that are changed between the two models.

https://doi.org/10.1371/journal.pcbi.1011940.g003

Model 2: SG viral inhibition by cytokines

While we observed a large increase of IE1-specific CD8 T cells within the SG, MHC I expression has been found to be suppressed in MCMV-infected SG cells, thereby preventing their recognition and direct killing [30]. However, significant expansion of activated CD4 T cells was also seen in the SG of infected mice (Fig 2D). As such, we developed a competing mathematical model consistent with elegant studies demonstrating that CD4 T cell-mediated cytokine release, principally IFN-γ, is critical for inhibiting MCMV replication in the SG (28,31–33). Our data and others suggest that this mechanism is far more important in the SG than in other parts of the body [30], where we found a less pronounced expansion of activated CD4 T cells compared to activated CD8 or NK cells over the course of infection.

To incorporate the immunological mechanism of cytokines into the model, we supposed that cytokines are produced by CD4+ T cells following the initiation of infection, and lead to a time-dependent inhibition of viral production within infected SG cells, represented by $f(t)$. This function takes on values between 0 and 1 and directly scales parameter p_1 to represent infected cells entering an antiviral state due to the presence of cytokines and thereby reducing their rate of viral production. We assume $f(t)$ takes on the form

$$f(t) = 1 - \frac{y\,t}{z + t} \tag{2}$$

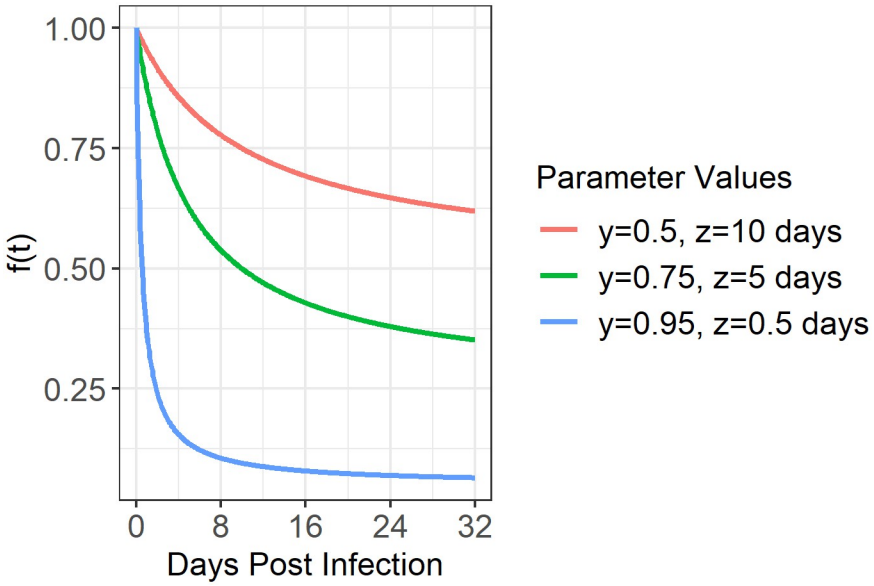

Fig 4. Sketch plot of function *f*(*t*) that inhibits viral production in the SG. ***f*(*t*)**, taking the form of $\boldsymbol{f(t) = 1 - \frac{yt}{z+t}}$, is assumed to directly scale the production of virus in the SG (parameter $\boldsymbol{p_1}$) as a function of days post infection (***t***). This scaling represents the entry of infected cells into an antiviral state due to the increasing presence of cytokines and thus a decrease in their rate of viral production. Parameters ***y*** and ***z*** are fit to data, with examples of ***f*(*t*)** for different values of ***y*** and ***z*** shown here.

https://doi.org/10.1371/journal.pcbi.1011940.g004

where y and z are parameters fit to data. This equation draws from Michaelis-Menten kinetics, where as time increases, we assume so does the presence of cytokines, and thus $f(t)$ approaches 0. In establishing the form of $f(t)$, we did model fits to versions where the effect of cytokines later dropped, due to the assumption that SG infected cells would eventually no longer be in an antiviral state, however, there was no evidence of such a change over the course of time considered. A sketch plot of how $f(t)$ behaves for different values of y and z appears in Fig 4.

Due to suppression of MHC I expression on infected SG cells [30], we also assumed that these cells (I_s) are no longer targeted by CD8 T cells (T). As the literature does not point to a direct role of CD4 T cells in controlling MCMV infection elsewhere in the body, the model assumes the effect of cytokines is limited to the SG. Equation set (3) shows the full set of ODEs for Model 2. A visual representation is again provided in Fig 3.

$$\begin{aligned}
\frac{dI_s}{dt} &= \eta_1 V_s - \delta I_s \\
\frac{dV_s}{dt} &= p_1 f(t) I_s - c V_s - \mu_1 V_s + \mu_2 V_b \\
\frac{dI_b}{dt} &= \eta_2 V_b - \delta I_b - m_2 I_b T \\
\frac{dV_b}{dt} &= p_2 I_b - c V_b - \mu_2 V_b + \mu_1 V_s \\
\frac{dT}{dt} &= \alpha \frac{I_b + I_s}{I_b + I_s + w} - dT
\end{aligned} \tag{3}$$

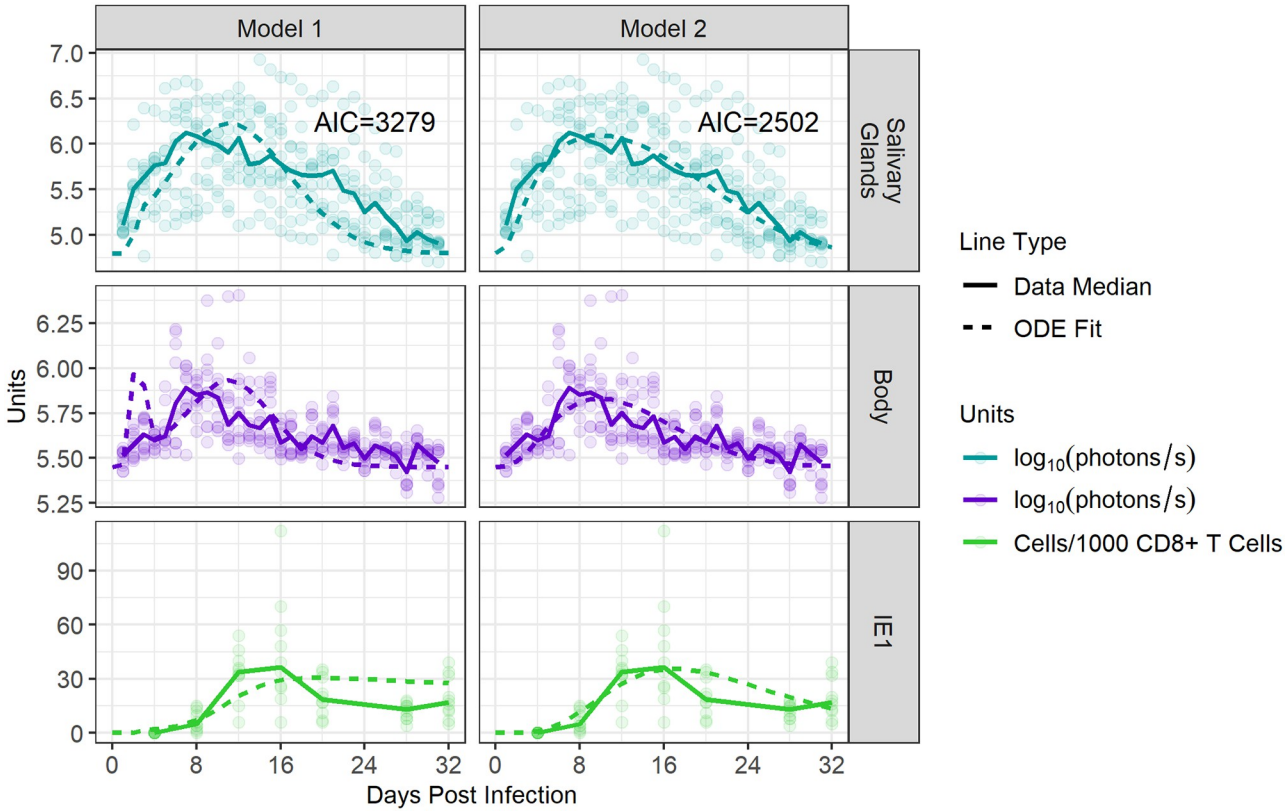

Fig 5. Control of viral replication in the SG is better explained by CD4 T cell-mediated cytokine production than direct killing by CD8 T cells. We compared how well each mathematical model was able to reproduce the observed murine data. Simultaneous fits for each model across 10 mice are shown. Dots represent luminescent signals captured in the SG and body during bioimaging and the number of IE1-specific CD8 T cells/1000 CD8 T cells within the blood. Solid lines indicate median values. Dotted lines show the optimal ODE fit, as determined by our fitting algorithm. AIC values for each model are shown.

https://doi.org/10.1371/journal.pcbi.1011940.g005

CD8 T cell killing of infected cells does not explain the control of MCMV replication in the SG

We fit each mathematical model to pooled data from 10 ISG infected mice over 32 days post-infection, to test how well each model describes the data. Specifically, we fit V_s to bioimaging signals in the SG, V_b to bioimaging signals in the body, and T to the size of the IE1-specific CD8 T cell population in the blood (see the Methods section for details). We specifically used data from blood to fit T as were able to collect frequent longitudinal blood samples from mice, unlike from spleen or SG. We also assumed a linear relationship between bioimaging signals and pfu, as has been described [18,42,43]. During fitting, parameters with known values in the literature, or those that could not be distinguished during fitting, were left fixed, while others were allowed to vary. As such, parameters m_1, m_2, α, d, η_1, η_2, y, p_1, p_2, w, and z were fit while δ, and c were kept constant. As the gating area of the body was 4.54 times the size of the gating area of the SG, μ_1 was assumed to equal $4.54\mu_2$, and μ_2 was fit. Results of these fits are shown in Fig 5. The two model fits were compared using the Akaike information criterion (AIC), which evaluates the prediction error of each model. Consistent with experimental observations [20,30–32], Model 2 (CD4 T cell-derived IFN-γ) outperformed Model 1 (direct killing by IE1-specific CD8 T cells) with a ΔAIC of 777. With such a large ΔAIC, these results indicate that Model 2 better explains the data and that control of salivary gland infection is attributable

more to the inhibition of viral production by cytokines, rather than to IE1-specific T cells as in Model 1. In particular, Model 2 better captured the fast rise in viral load (VL) observed in experiments. Thus, all further data analyses were performed using Model 2.

We next fit Model 2 to data from each infected mouse to arrive at one set of best-fitting parameter values for each animal. Examples of individual fits are shown in Fig 6A, and the general trend seen over time for all model compartments is shown in Fig 6B. Remaining fits for other ISG-infected mice are shown in Fig C in S1 Text. We found that the time-dependent function $f(t)$ meant to represent the damping of viral production within the SG due to the presence of cytokines quickly approached values close to 0, indicating the importance of a fast and long-lasting effect of cytokines on viral control within the SG (Fig 6B). The median value and 5–95% quantiles for each fit parameter when pooling all fits are shown in Table 1.

Having generated estimates of all parameter values in our model, we next compared how parameter values governing the infection dynamics within the SG and the rest of the body differ and estimated how quickly MCMV is exchanged between these compartments. Our model predicts that the production rate of virus within the SG, p_1, is significantly faster than the production rate of virus within the body, p_2, (p-value$<$0.05) coinciding with the high luminescence signals observed in the SG. We also noted that the exchange of virus from the body to the SG and from the SG to the body is quite fast, occurring at a median rate of $\mu_2 = 0.497$/day and $\mu_1 = 4.54\mu_2 = 2.26$/day, respectively, which corresponds to a half-life of residency of approximately 48 hours and 11 hours, respectively. While the rate at which virus causes new cellular infection in the SG (η_1) is faster than the rate at which virus causes new cellular infection in the body (η_2), this difference was not significant.

Mathematical modelling predicts a high within-host basic reproductive number for MCMV

Using the estimated parameter values, we calculated the within-host basic reproductive number (R_0) for MCMV in the SG. Here, R_0 is defined as the number of infected cells propagated by a single infected cell in the absence of any immunity. For our mathematical model, R_0 is defined as the dominant eigenvalue of the model's next generation matrix [45], and equals

$$R_0 = \frac{\mu_2 p_1 \eta_1}{(\mu_1 + \mu_2)2\delta c} + \frac{\mu_1 p_2 \eta_2}{(\mu_1 + \mu_2)2\delta c}$$

Calculating R_0 using our fit parameter values gave a median R_0 value of 3.8 (5–95% quantiles of 2.3–8.0). As a point of comparison, the within-host infection R_0 value was estimated to be 1.6 for HCMV using clinical data obtained during infant primary infections [24].

Low-dose primary SG infections in mice are predicted to persist and spread

To conclude our mathematical analysis of MCMV dynamics in the SG, we used our model to predict the relationship between the ISG inoculum and viral spread. By simulating the stochastic analogue of the system of ODEs described in Model 2 and using parameter values obtained through fitting (Table 1), we varied the initial dose assumed to be injected into the SG. Though this analysis, we identified which inoculation doses are predicted to result in persistent SG replication and systemic dissemination, and which inoculations may cause brief self-limited SG infection. Results are shown in Fig 7A.

Our model predicts that with a dose of 14 PFU of K181-luc administered ISG, 50% of mice will have a sustained infection that disseminates throughout the body (ID_{50}; Fig 7A). At doses of 50 PFU, and 75 PFU, our model predicts that 94% and 99% of mice, respectively, would have a systemic infection.

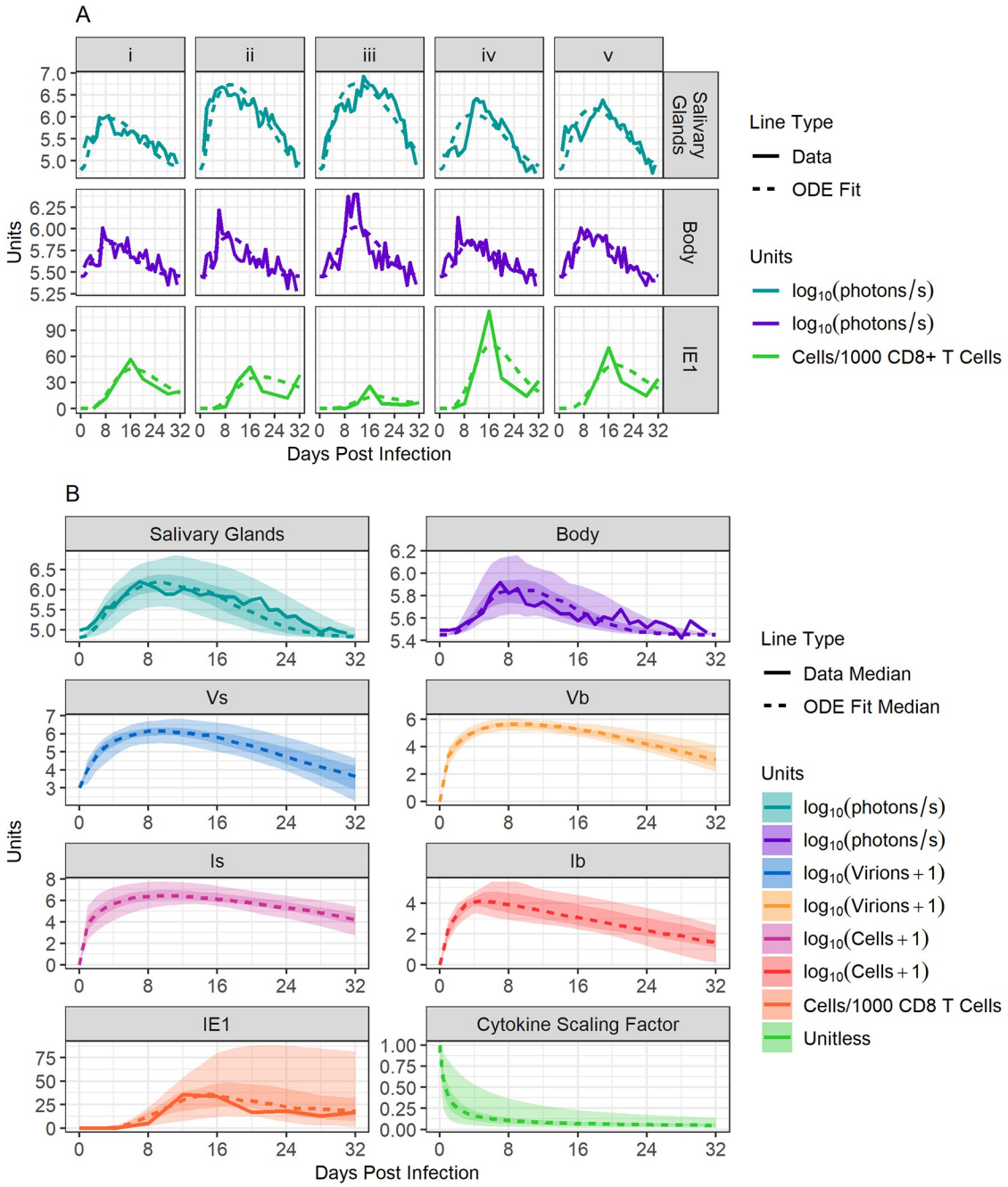

Fig 6. Mathematical modelling of primary MCMV infection. Panel A: Model 2 fit, with data from 5 mice separately. "Salivary Glands" represents the amount of luminescent signal detected in the SG, "Body" represents the amount of luminescent signal detected in the body, and "IE1" represents the number of virus-specific CD8+ T cells seen in the blood. **Panel B**: Summary of fits for all mice and for all compartments of the model. Dotted lines show the median value of best fitting simulations, while solid lines show the median value of collected data (when a comparison was available). Dark ribbons show the 25–75% quantiles and light ribbons show the 5–95% quantiles. The "Cytokine Scaling Factor" sub-panel shows the dynamics of function $f(t)$.

https://doi.org/10.1371/journal.pcbi.1011940.g006

Our model also predicts that transient SG infection, with limited viral replication within the SG that dies out before spreading to the rest of the body (Fig 7B and 7C) is possible with low-PFU inoculations. However, transient infections are still predicted to be rare, occurring most frequently with a ISG inoculation of 11 PFU in 5% of inoculations. When a transient

Table 1. Parameters used in the mathematical model. Numbers marked with a (*) indicate parameters that were estimated by fitting Model 2 to data. (+) indicates the number was estimated based on values in the literature to determine the best value to match the kinetics of infection and kept constant during fitting.

Parameter	Description	Units	Literature Values	Estimate
p_1	Production rate of viruses by infected cells in the SG	day^{-1}	9.84–1600 [20,33]	1.14×10^{1}* (9.00, 1.74×10^2)
p_2	Production rate of viruses by infected cells in the body	day^{-1}	9.84–1600 [20,33]	2.36×10^{1}* ($9.38,4.91\times10^{1}$)
m_2	Rate at which T kill I_b via mass action	day^{-1}	0.01 [44]	1.72* (3.85×10^{-2},4)
α	Maximum rate at which I_b and I_s stimulate production of T	day^{-1}	___	1.12×10^{3}* (1.23×10^{2}, 9.53×10^{3})
d	Death rate of T	day^{-1}	0.05–0.322 [15,44]	6.77×10^{-2}* (1.00×10^{-2}, 2.93×10^{-1})
μ_2	Rate of viral exchange from body to SG	day^{-1}	___	4.97×10^{-1}* ($1.06\times10^{-1}2.37$)
η_1	Rate at which V_s causes new cellular infection	day^{-1}	0.6 [44]	2.69* (3.82×10^{-1}, 3.05×10^{1})
η_2	Rate at which V_b causes new cellular infection	day^{-1}	0.6 [44]	3.51×10^{-1}* (1.39×10^{-1}, 9.41×10^{-1})
w	Number of infected cells needed for T cell production to reach its half-max rate	*cells*	___	7.30×10^{8}* (7.81×10^{7}, 7.01×10^{9})
y	Maximum factor at which viral production is inhibited due to the presumed presence of cytokines in the SG	*unitless*	___	0.97* (0.93–0.99)
z	Number of days post-infection when inhibition of viral production in SG reaches its half-max amount	*days*	___	5.96×10^{-1}* (1.49×10^{-1} – 2.84)
δ	Natural death rate of infected cells	day^{-1}	0.77–1.2[33,44]	1^{+}
c	Decay rate of viruses	day^{-1}	2–10.8 [20,33]	8.8^{+}
	Mean bioimaging background signal from bioimaging	$photons/s/cm^2/steradian$		1.57×10^{3}
	Bioimaging SG gating area	cm^2		3.13
	Bioimaging body gating area	cm^2		14.2

https://doi.org/10.1371/journal.pcbi.1011940.t001

infection does occur, a median of only 1 cell (5–95% quantile of 1–3 cells) within the SG is predicted to be infected at any time. These infections are also predicted to die out very quickly, only lasting a median of 0.7 days (5–95% quantiles of 0.3–4.4 days). This phenomenon is likely due to the predicted high rate of viral exchange between the SG and the rest of the body (μ_1) and a relatively high R_0 value, suggesting that once cells are infected in the SG, replication almost always persists, and typically also spreads rapidly to the rest of the body.

Fitting our mathematical model to other MCMV infection data

To validate our model, we next examined whether infections via the IP route with different inocula of MCMV were consistent with Model 2. Mice were infected with either a low (10^2 PFU) or a high (10^6 PFU) dose of K181-luc, imaged daily for luminescence, and blood samples were taken every seven days to measure changes in immune cell populations. Model 2 fit these new data well, reproducing the rise and fall in VL and immune cell population sizes. Data and fits from mice infected with 10^2 PFU IP and 10^6 PFU IP are shown in Fig D in S1 Text.

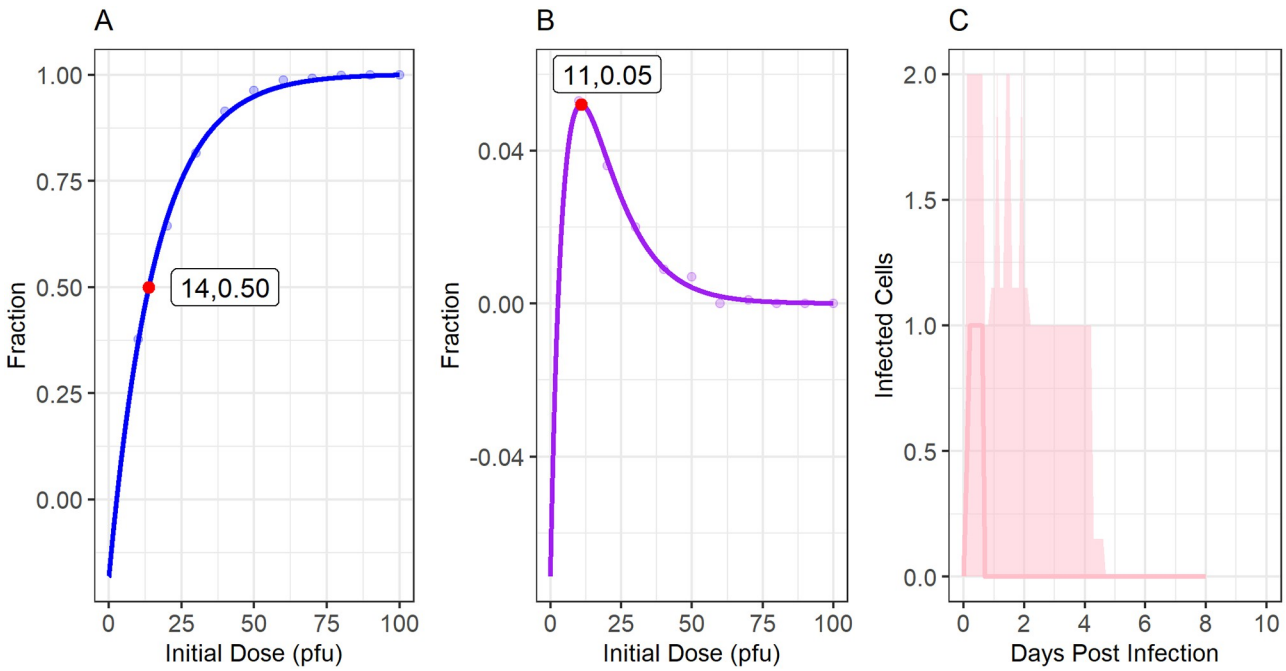

Fig 7. Modelled spread of SG infections in mice. Panel A: We modelled the fraction of SG infections that disseminate beyond the SG in mice as a function of the initial ISG dose. The red dot shows that our model predicts the ID_{50}, the ISG dose at which 50% of infections spread beyond the SG, to be 14 PFU. **Panel B**: The fraction of inoculations that cause transient local infection in the SG as a function of the initial dose. Here, a transient infection is one that infects SG cells but dies out before spreading to the body. As indicated by the red dot, our model predicts transient infection is most likely with an initial dose of 11 PFU, occurring after 5% of inoculations. **Panel C**: Our model's predictions on the number of infected cells among infections that are limited to the SG over time when inoculating mice with an ISG dose of 11 PFU. Among infections that do not disseminate, very few cells become infected (median maximum of 1 cell, 5–95% quantiles of 1–3 cells), and replication dies out very quickly, taking a median of 0.7 days (5–95% quantiles of 0.3–4.4 days) to be cleared. Lines in panels A and B show the line of best fit. The line in panel C indicates the median behaviour, and light ribbons show the 5–95% quantiles over time.

https://doi.org/10.1371/journal.pcbi.1011940.g007

Finally, we looked at how the parameter values predicted when fitting Model 2 to data from ISG inoculation versus IP inoculation compared. Distributions of fit parameters for each data set are shown in Fig 8. In general, estimated parameter values were similar with different ROA. Values for m_2, α, d, and y showed small but significant differences across data sets (Fig 8). The largest most significant differences were seen for parameter η_2, which was estimated to be significantly larger when fitting the model to data from IP infected mice than when fitting it to data from ISG infected mice.

Discussion

A deeper understanding of the kinetics and immune correlates of CMV SG replication has the potential to inform the design of vaccines to prevent infection and transmission. Through collecting comprehensive time-series data following a low dose ISG infection of MCMV in mice, we identified organ-specific fluctuations in key immune cell populations and their temporal relation to viral replication dynamics. Using these experimental data, we designed and fitted novel mathematical models describing the spatial spread of MCMV and the immune responses within different compartments of the body to glean insight into the determinants of systemic infection and immune control.

IE1-specific CD8 T cells expanded at the highest rate following infection. However, lasting and significant elevations in populations of KLRG1+ CD8 T cells, KLRG1+ NK cells, and

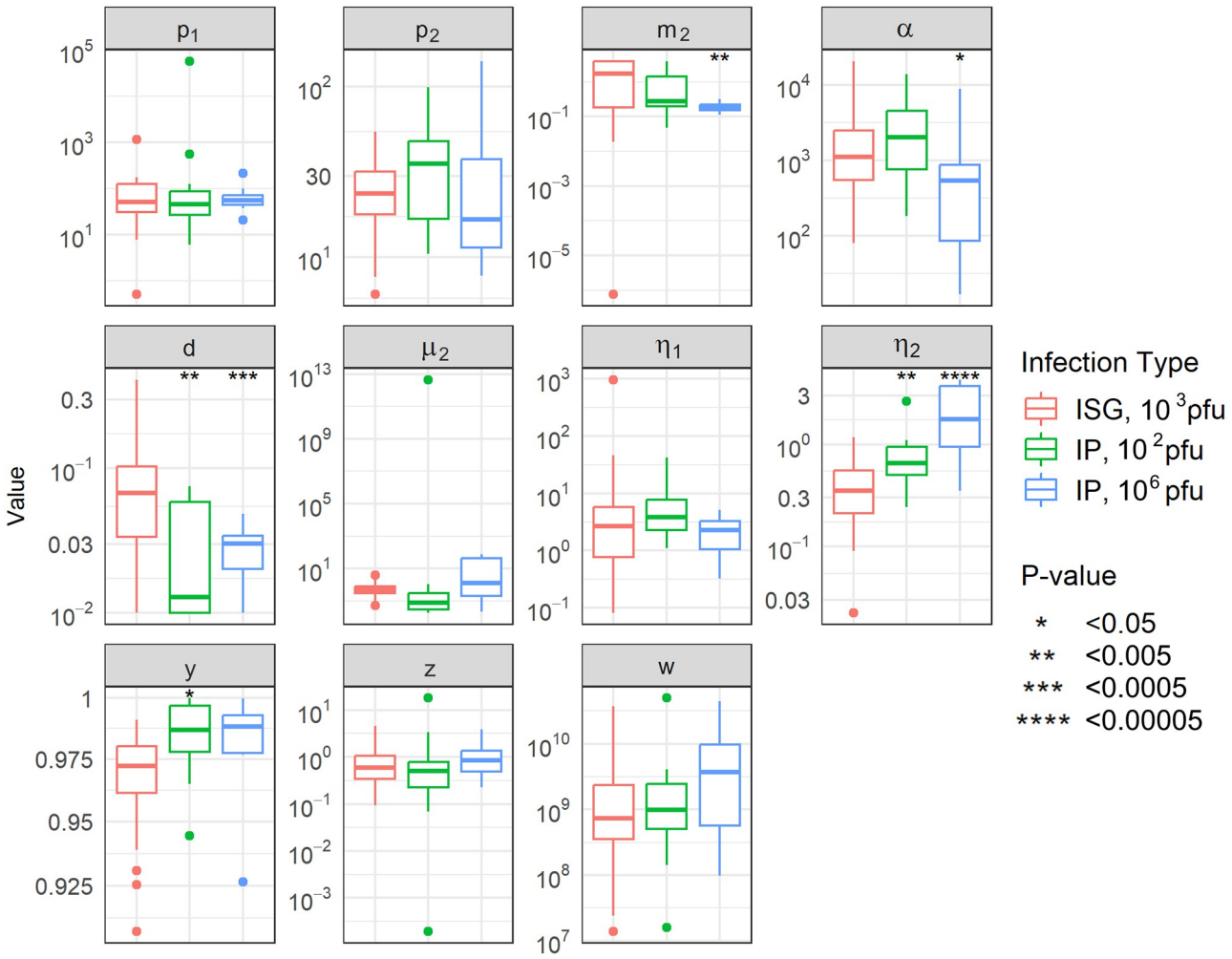

Fig 8. Parameter distributions for model fit parameters when fitting individual mouse data. Parameter distributions across the data sets were stratified to fit Model 2. Significant differences were seen between the "fit" of parameter values using ISG-infected mice and their fit using IP-infected mice.

https://doi.org/10.1371/journal.pcbi.1011940.g008

KLRG1+ CD4 T cells were also observed, eventually contracting with decreasing viral replication. We anticipated differences in immune cell dynamics according to anatomic compartment given the relatively greater and longer viral replication in SG. Indeed, virus luminescence rose three times faster during the early stages of infection and declined four times slower following signal peak in SG than the rest of the body. While weaker IE1-specific CD8 T cell and KLRG1+ NK cell responses were observed in SG than at other sites, all four immune cell populations generally displayed similar kinetics in all compartments. This suggests that despite the presence of similar immune cell populations at different anatomic sites, their ability to recognize and eliminate infected cells differs. One limitation to our model is that only data on IE1-specific CD8 T cells from blood were used rather than including those from the SG and spleen, which was chosen because blood allowed frequent and longitudinal sampling without sacrifice. However, differences in the abundance of this cell type within each compartment was not reflected and could potentially explain some of viral dynamics observed. In support of other

studies [20,30–32], our mathematical analysis suggested that killing of infected cells by virus-specific CD8 T cell is sufficient to explain viral kinetics only outside the SG. In contrast, the model requires cytokine production by CD4 T cells in the SG to accurately reproduce the experimental data.

Our mouse model used small amounts of virus delivered via ISG in an attempt to mimic human infection, which allowed us to characterize the rate of persistence and spread within and beyond the SG. Oral HCMV infection may at times die out before causing a full systemic infection, based on prospective cohort data, in which brief, low-level episodes of viral shedding in saliva can be observed in individuals in the absence of seroconversion [10,33,46,47]. Self-limited local infections appear to be due to a low within-host R_0 for HCMV, estimated at 1.6 in the infant oral cavity and thus quite poor cell-to-cell spread of infection in the oral mucosal epithelium [33]. In contrast, our mathematical model estimates an R_0 of 3.8 for MCMV in the SG of our experimental animals. Further, while previous research has suggested that ISG ROA of MCMV leads to reduced systemic pathology as compared to other ROAs [13], our model suggested viral spread from the SG to the rest of the body is still quick and efficient, such that self-limited SG infections are rare and last only 1–2 days.

The observation that MCMV disseminates more efficiently than HCMV may simply represent intrinsic differences in these viruses, given that MCMV replication lasts days-weeks after primary infection compared to weeks-months for HCMV [24] Importantly, the efficiency of viral spread measured using the MCMV strain K181, which is highly laboratory adapted, may not reflect wild-type strains. Further, we cannot rule out the possibility that direct injection into mouse SG tissue in the mouse differs from natural oral HCMV acquisition. For example, trauma resulting from ISG inoculation could have could favour faster spread to other anatomic sites. In addition, other oral epithelial cell types may be infected prior to SG in humans. HCMV infection is often acquired early in life as a result of frequent, repeated exposures [48–50], as opposed to a single inoculation into the SG. Breast milk, a common source of infection in infants, also contains a host of antibodies and other immune factors that may influence the likelihood and course of infection [51,52]. Further, while the SG is indisputably a site of early viral infection in both humans and mice [14,16,18], elegant studies indicate that natural infection in the mouse is likely acquired through the nose [17,23,53]. Thus, future models should be informed by experimental infections employing intranasal inoculation or breast milk transmission.

Our results also bear significant relevance for the design of vaccines aimed at preventing infection or minimizing shedding [10,54], and thereby curbing transmission to pregnant women, an approach that appears highly effective in preventing cCMV [55–57]. By revealing the unique persistence of viral replication within the salivary glands despite the presence of similar infection-induced immune cells to those observed in the rest of the body, our findings underscore a critical point: the requirements for a vaccine to confer protection or minimize shedding in the salivary glands likely differ significantly from those needed at other bodily sites. With the probable importance of the salivary glands in oral transmission, both as a site of initial exposure and as a contributor to the amount of virus shed into saliva, this aspect may become a crucial component in the design of a successful vaccine. Consequently, vaccine strategies emphasizing the stimulation of IFN-γ and TNF-α, which appear necessary for salivary gland CMV control, rather than simply a robust CD8 T cell response, may emerge as essential requirements for preventing or mitigating the duration and severity of infection.

Materials and methods

Ethics statement

All mouse work was performed at the Animal Care Facility at The British Columbia Children's Hospital Research Institute and was approved by the University of British Columbia Animal Care Committee (protocol numbers A19-0154, A19-0093, A15-0077).

Virus and inoculation of mice

Female BALB/c mice obtained from Charles River were infected with a variant of the K181 strain of MCMV with the *m78* gene tagged with luciferase (generously gifted by Helen Farrell, University of Queensland). A full description of this construct has been described elsewhere [18]. Virus stocks were grown in M2-10B4 cells (ATCC # CRL-1972) with RPMI 1640 Medium special formulation (Thermo Fisher cat # A1049101) supplemented with 10% fetal bovine serum (Thermo Fisher cat # 12483020) and 1% penicillin-streptomycin (Thermo Fisher cat # 15140148). Mice were infected via ISG or IP administration. For ISG administration, a 5 μl solution containing 1000 PFU of K181-luc and PBS was prepared and injected with a syringe directly into the right submandibular SG while the mouse was under isoflurane anasthesia. Preliminary tests performed indicated this to be the lowest dose necessary to ensure infection of all mice following ISG inoculation. For IP inoculation, a 100 μl solution containing either 10^2 PFU or 10^6PFU of K181-luc was diluted in PBS and injected with a syringe directly into the peritoneum of mice while they were awake and scruffed. All mice were between the ages of 6 and 10 weeks when inoculated. A total 39 mice were infected ISG with 1000 PFU, 11 mice were infected IP with 100 PFU, and 11 mice were infected IP with 10^6 PFU. For every infected mouse, a control mouse was administered PBS, either ISG or IP, and monitored at the same time and treated in the same way as infected mice.

Bioimaging

Mice received an IP injection of 100 μl of a 2% D-luciferin solution (Goldbio cat # 115144-35-9), were anaesthetized with isoflurane gas, and transferred to a Spectral Instruments Ami HTX bioimager for monitoring of light emission with a CCD camera. Bioimaging data was analyzed using the Aura Image Analysis software.

Tissue and blood sample collection and flow cytometry

Blood was collected from mice via the saphenous vein every four days for mice infected via ISG administration, and every seven days for mice infected via IP administration. Spleens and SG were harvested every eight days from subsets of ISG infected mice. Spleens were homogenized and strained through a 70 μm mesh to yield a single-cell suspension. SG were processed using the MACS Miltenyi multi-tissue dissociation kit (order no. 130-110-201) to create a single-cell suspension. Blood and spleen cell suspensions were further incubated with an RBC lysis buffer (eBioscience, cat # 00-4300-54). Single-cell suspensions were then stained with eFluor 780-conjugated viability dye (Invitrogen eBioscience cat # 65-0865-14), and fluorescently tagged with monoclonal antibodies against CD3 (PerCP-eFluor 710, eBioscience cat # 46-0032-82), CD19 (BV-510, BioLegend, cat # 115545), CD4 (BV-785, BioLegend cat # 100453), CD8a (BUV-737, BD Bioscience cat # 564297), gd (BUV-563, BD Bioscience cat # 748993), CD69 (PE-CF594, BD Bioscience cat # 562455), KLRG1 (APC, BioLegend cat # 138411), CD335 (BV-711, BD Bioscience cat # 740822), CD49b (PE-Cyanine7, eBioscience cat # 12-5971-82), and MHC class I tetramer containing the FITC-labelled H-2L^d 168-YPHFMPTNL-176 peptide produced by the *ie1* MCMV gene (obtained from the NIH

Tetramer facility core). Cells were analyzed for the presence of fluorophores using the BD FACSymphony flow cytometer. Flow cytometry data was analyzed and gated using FlowJo software.

Statistical analysis

Statistical significance of differences between data from infected and uninfected mice at specific time points was determined using the Mann-Whitney test. *P*-values less than 0.05 were considered statistically significant. Rates of exponential growth and decay of immune cell populations and luminescent signals were analysed by fitting a linear model to the number of days post-infection and the log-transformed data. For exponential growth, only data points collected before the median peak value were included. For exponential decay, only data points collected after the median peak value were included.

Model simulation and parameter estimation

Mathematical models were simulated using the R package, "pomp" [58]. Parameters of the model were fit by matching the trajectories of the deterministic model to our data. Here, we chose distributions to determine the probability of model predictions given the observed data and used these to create a likelihood function. We then created an objective function meant to evaluate the likelihood function and used the Nelder-Mead method to search parameter space to find parameters that maximized this likelihood. Throughout fitting, we kept parameters δ and c fixed while allowing all other parameters defined in the set of ODEs to vary.

Defining the likelihood function

Let $V_b(t)$ be the model-predicted number of virions present in the body at time t, a be the measured number of photons/s released per virion, B_b be the average background signal in the body as measured in uninfected mice, and $M_b(t)$ be the bioimaging signal measured in the body at time t in units of photons/s. We then assume $aV_b(t) + B_b$ follows a lognormal distribution with mean $M_b(t)$ and standard deviation ρ_1.

Similarly, letting $V_s(t)$ be the number of virions present in the SG at time t, B_s be the average background signal in the salivary gland, and $M_s(t)$ be the bioimaging signal measured in the SG at time t in units of photons/s, we assume $aV_s(t) + B_s$ follows a lognormal distribution with mean $M_s(t)$ and standard deviation ρ_1.

For comparing model predicted numbers of IE1-specific CD8 T cells to data, we let T(t) be the model-predicted number of T cells in the blood at time t, f be the average number of CD8 T cells in the blood, ρ_2 be a cell's probability of being observed through flow cytometry, and $F_{IE1}(t)$ be the measured fraction of CD8 T cells that are IE1-specific in the blood at time t. Thus, we assume $T(t)$ follows a Poisson distribution with rate $\rho 2 f F_{IE1}(t)$.

With these assumptions, we define the likelihood function as

$$
\begin{aligned}
&Likelihood = \\
&\sum_{\forall t \in V_{b,t}} \frac{1}{(aV_b(t) + B_b)\rho_1\sqrt{2\pi}} \exp\left(-\frac{(\ln(aV_b(t) + B_b) - \mathrm{M_b}(t))^2}{2\rho_1^2}\right) + \\
&\sum_{\forall t \in V_{s,t}} \frac{1}{(aV_s(t) + B_s)\rho_1\sqrt{2\pi}} \exp\left(-\frac{(\ln(aV_s(t) + B_s) - \mathrm{M_s}(t))^2}{2\rho_1^2}\right) + \\
&\sum_{\forall t \in T_t} \frac{(\rho_2 f F_{IE1}(t))^{T(t)} \exp(-\rho_2 f F_{IE1}(t))}{T(t)!}
\end{aligned}
$$

where $V_{b,t}$ is the set of times where M_b was measured, $V_{s,t}$ is the set of times where M_s was measured and T_t is the set of times F_{IE1} was measured.

Stochastic simulations

Stochastic simulations of the model were performed by converting the deterministic skeleton of the mathematical model into a series of individual reactions. The model progresses through time following the tau-leaping algorithm where small time steps of 0.001 days were made [59]. At each time step, the number and type of reactions occurring were randomly chosen from a Poisson or Multinomial distribution, depending on the independence of the reaction, with the probability dependent on the reaction rate.

Supporting information

S1 Text. Supplementary figures.
(PDF)

Author Contributions

Conceptualization: Catherine M Byrne, Daniel Coombs, Soren Gantt.

Data curation: Catherine M Byrne.

Formal analysis: Catherine M Byrne, Daniel Coombs.

Funding acquisition: Soren Gantt.

Investigation: Catherine M Byrne, Ana Citlali Márquez, Bing Cai.

Methodology: Catherine M Byrne, Ana Citlali Márquez, Bing Cai.

Project administration: Ana Citlali Márquez, Bing Cai, Soren Gantt.

Resources: Bing Cai, Soren Gantt.

Supervision: Daniel Coombs, Soren Gantt.

Writing – original draft: Catherine M Byrne.

Writing – review & editing: Catherine M Byrne, Ana Citlali Márquez, Bing Cai, Daniel Coombs, Soren Gantt.

References

1. Cannon MJ, Schmid DS, Hyde TB. Review of cytomegalovirus seroprevalence and demographic characteristics associated with infection. Rev Med Virol. 2010; 20: 202–213. https://doi.org/10.1002/rmv.655 PMID: 20564615
2. Johnston C, Orem J, Okuku F, Kalinaki M, Saracino M, Huang M-L, et al. HIV-1 infection is associated with increased frequency of mucosal and plasma cytomegalovirus & Epstein-Barr virus detection in Ugandan adults. unpublished. 2014.
3. Gantt S, Orem J, Krantz EM, Morrow RA, Selke S, Huang M-L, et al. Prospective characterization of the risk factors for transmission and symptoms of primary human herpesvirus infections among Ugandan infants. J Infect Dis. 2016; 214: 36–44. https://doi.org/10.1093/infdis/jiw076 PMID: 26917575
4. Ssentongo P, Hehnly C, Birungi P, Roach MA, Spady J, Fronterre C, et al. Congenital cytomegalovirus infection burden and epidemiologic risk factors in countries with universal screening: a systematic review and meta-analysis. JAMA Netw Open. 2021; 4: e2120736. https://doi.org/10.1001/jamanetworkopen.2021.20736 PMID: 34424308
5. Cannon MJ, Hyde TB, Schmid DS. Review of cytomegalovirus shedding in bodily fluids and relevance to congenital cytomegalovirus infection. Rev Med Virol. 2011; 21: 240–255. https://doi.org/10.1002/rmv.695 PMID: 21674676

6. Britt WJ. Human cytomegalovirus infection in women with preexisting immunity: sources of infection and mechanisms of infection in the presence of antiviral immunity. J Infect Dis. 2020; 221: S1–S8. https://doi.org/10.1093/infdis/jiz464 PMID: 32134479
7. Plotkin SA. Preventing infection by human cytomegalovirus. J Infect Dis. 2020; 221: S123–S127. https://doi.org/10.1093/infdis/jiz448 PMID: 32134484
8. Johnson J, Anderson B, Pass RF. Prevention of maternal and congenital cytomegalovirus infection. Clin Obstet Gynecol. 2012; 55: 521–530. https://doi.org/10.1097/GRF.0b013e3182510b7b PMID: 22510635
9. Griffiths PD, McLean A, Emery VC. Encouraging prospects for immunisation against primary cytomegalovirus infection. Vaccine. 2001; 19: 1356–1362. https://doi.org/10.1016/s0264-410x(00)00377-7 PMID: 11163656
10. Das R, Blázquez-Gamero D, Bernstein DI, Gantt S, Bautista O, Beck K, et al. Safety, efficacy, and immunogenicity of a replication-defective human cytomegalovirus vaccine, V160, in cytomegalovirus-seronegative women: a double-blind, randomised, placebo-controlled, phase 2b trial. Lancet Infect Dis. 2023; S1473-3099(23)00343–2. https://doi.org/10.1016/S1473-3099(23)00343-2 PMID: 37660711
11. Pass RF, Zhang C, Evans A, Simpson T, Andrews W, Huang M-L, et al. Vaccine prevention of maternal cytomegalovirus infection. N Engl J Med. 2009; 360: 1191–1199. https://doi.org/10.1056/NEJMoa0804749 PMID: 19297572
12. Byrne C, Coombs D, Gantt S. Modestly protective cytomegalovirus vaccination of young children effectively prevents congenital infection at the population level. Vaccine. 2022; 40: 5179–5188. https://doi.org/10.1016/j.vaccine.2022.07.026 PMID: 35907677
13. Pilgrim MJ, Kasman L, Grewal J, Bruorton ME, Werner P, London L, et al. A focused salivary gland infection with attenuated MCMV: An animal model with prevention of pathology associated with systemic MCMV infection. Exp Mol Pathol. 2007; 82: 269–279. https://doi.org/10.1016/j.yexmp.2006.12.010 PMID: 17320076
14. Grewal JS, Pilgrim MJ, Grewal S, Kasman L, Werner P, Bruorton ME, et al. Salivary glands act as mucosal inductive sites via the formation of ectopic germinal centers after site-restricted MCMV infection. FASEB J. 2011; 25: 1680–1696. https://doi.org/10.1096/fj.10-174656 PMID: 21307334
15. Gabel M, Baumann NS, Oxenius A, Graw F. Investigating the dynamics of MCMV-specific CD8+ T cell responses in individual hosts. Front Immunol. 2019; 10. https://doi.org/10.3389/fimmu.2019.01358 PMID: 31281313
16. Liu G, Zhang F, Wang R, London L, London SD. Protective MCMV immunity by vaccination of the salivary gland via Wharton's duct: replication-deficient recombinant adenovirus expressing individual MCMV genes elicits protection similar to that of MCMV. FASEB J. 2014; 28: 1698–1710. https://doi.org/10.1096/fj.13-244178 PMID: 24391133
17. Farrell HE, Lawler C, Tan CSE, MacDonald K, Bruce K, Mach M, et al. Murine cytomegalovirus exploits olfaction to enter new hosts. mBio. 2016; 7: e00251–16. https://doi.org/10.1128/mBio.00251-16 PMID: 27118588
18. Farrell H, Oliveira M, Macdonald K, Yunis J, Mach M, Bruce K, et al. Luciferase-tagged wild-type and tropism-deficient mouse cytomegaloviruses reveal early dynamics of host colonization following peripheral challenge. J Gen Virol. 2016; 97: 3379–3391. https://doi.org/10.1099/jgv.0.000642 PMID: 27902356
19. Trgovcich J, Kincaid M, Thomas A, Griessl M, Zimmerman P, Dwivedi V, et al. Cytomegalovirus reinfections stimulate CD8 T-memory inflation. PLOS ONE. 2016; 11: e0167097. https://doi.org/10.1371/journal.pone.0167097 PMID: 27870919
20. Oderbolz J, Zangger N, Zimmermann L, Sandu I, Starruß J, Graw F, et al. Locally confined IFNγ production by CD4+ T cells provides niches for murine cytomegalovirus replication in the salivary gland. bioRxiv. 2021; 01.14.426650. https://doi.org/10.1101/2021.01.14.426650
21. Rawlinson WD, Farrell HE, Barrell BG. Analysis of the complete DNA sequence of murine cytomegalovirus. J Virol. 1996; 70: 8833–8849. https://doi.org/10.1128/JVI.70.12.8833-8849.1996 PMID: 8971012
22. Krmpotic A, Bubic I, Polic B, Lucin P, Jonjic S. Pathogenesis of murine cytomegalovirus infection. Microbes Infect. 2003; 5: 1263–1277. https://doi.org/10.1016/j.micinf.2003.09.007 PMID: 14623023
23. Oduro JD, Redeker A, Lemmermann NAW, Ebermann L, Marandu TF, Dekhtiarenko I, et al. Murine cytomegalovirus (CMV) infection via the intranasal route offers a robust model of immunity upon mucosal CMV infection. J Gen Virol. 2016; 97: 185–195. https://doi.org/10.1099/jgv.0.000339 PMID: 26555192
24. Mayer BT, Matrajt L, Casper C, Krantz EM, Corey L, Wald A, et al. Dynamics of persistent oral cytomegalovirus shedding during primary infection in Ugandan infants. J Infect Dis. 2016; 214: 1735–1743. https://doi.org/10.1093/infdis/jiw442 PMID: 27651417

25. Cannon MJ, Stowell JD, Clark R, Dollard PR, Johnson D, Mask K, et al. Repeated measures study of weekly and daily cytomegalovirus shedding patterns in saliva and urine of healthy cytomegalovirus-seropositive children. BMC Infect Dis. 2014; 14: 569. https://doi.org/10.1186/s12879-014-0569-1 PMID: 25391640

26. Matrajt L, Gantt S, Mayer BT, Krantz EM, Orem J, Wald A, et al. Virus and host-specific differences in oral human herpesvirus shedding kinetics among Ugandan women and children. Sci Rep. 2017; 7: 13105. https://doi.org/10.1038/s41598-017-12994-0 PMID: 29026166

27. Stowell JD, Mask K, Amin M, Clark R, Levis D, Hendley W, et al. Cross-sectional study of cytomegalovirus shedding and immunological markers among seropositive children and their mothers. BMC Infect Dis. 2014; 14: 568. https://doi.org/10.1186/s12879-014-0568-2 PMID: 25388365

28. Lu X, Pinto AK, Kelly AM, Cho KS, Hill AB. Murine cytomegalovirus interference with antigen presentation contributes to the inability of CD8 T cells to control virus in the salivary gland. J Virol. 2006; 80: 4200–4202. https://doi.org/10.1128/JVI.80.8.4200-4202.2006 PMID: 16571839

29. Thom JT, Weber TC, Walton SM, Torti N, Oxenius A. The salivary gland acts as a sink for tissue-resident memory CD8 + T cells, facilitating protection from local cytomegalovirus infection. Cell Rep. 2015; 13: 1125–1136. https://doi.org/10.1016/j.celrep.2015.09.082 PMID: 26526997

30. Walton SM, Mandaric S, Torti N, Zimmermann A, Hengel H, Oxenius A. Absence of cross-presenting cells in the salivary gland and viral immune evasion confine cytomegalovirus immune control to effector CD4 T cells. PLOS Pathog. 2011; 7: e1002214. https://doi.org/10.1371/journal.ppat.1002214 PMID: 21901102

31. Lucin P, Jonjić S, Messerle M, Polić B, Hengel H, Koszinowski UH. Late phase inhibition of murine cytomegalovirus replication by synergistic action of interferon-gamma and tumour necrosis factor. J Gen Virol. 1994; 75 (Pt 1): 101–110. https://doi.org/10.1099/0022-1317-75-1-101 PMID: 8113718

32. Pavić I, Polić B, Crnković I, Lucin P, Jonjić S, Koszinowski UH. Participation of endogenous tumour necrosis factor alpha in host resistance to cytomegalovirus infection. J Gen Virol. 1993; 74: 2215–2223. https://doi.org/10.1099/0022-1317-74-10-2215 PMID: 8105025

33. Mayer BT, Krantz EM, Swan D, Ferrenberg J, Simmons K, Selke S, et al. Transient oral human cytomegalovirus infections indicate inefficient viral spread from very few initially infected cells. J Virol. 2017; 91. https://doi.org/10.1128/JVI.00380-17 PMID: 28381570

34. Karrer U, Sierro S, Wagner M, Oxenius A, Hengel H, Koszinowski UH, et al. Memory inflation: continuous accumulation of antiviral CD8+ T cells over time. J Immunol. 2003; 170: 2022–2029. https://doi.org/10.4049/jimmunol.170.4.2022 PMID: 12574372

35. Gründemann C, Schwartzkopff S, Koschella M, Schweier O, Peters C, Voehringer D, et al. The NK receptor KLRG1 is dispensable for virus-induced NK and CD8+ T-cell differentiation and function in vivo. Eur J Immunol. 2010; 40: 1303–1314. https://doi.org/10.1002/eji.200939771 PMID: 20201037

36. Huntington ND, Tabarias H, Fairfax K, Brady J, Hayakawa Y, Degli-Esposti MA, et al. NK cell maturation and peripheral homeostasis is associated with KLRG1 up-regulation. J Immunol. 2007; 178: 4764–4770. https://doi.org/10.4049/jimmunol.178.8.4764 PMID: 17404256

37. Fogel LA, Sun MM, Geurs TL, Carayannopoulos LN, French AR. Markers of nonselective and specific NK cell activation. J Immunol Baltim Md 1950. 2013; 190: 6269–6276. https://doi.org/10.4049/jimmunol.1202533 PMID: 23656738

38. Mitrović M, Arapović J, Jordan S, Fodil-Cornu N, Ebert S, Vidal SM, et al. The NK cell response to mouse cytomegalovirus infection affects the level and kinetics of the early CD8+ T-cell response. J Virol. 2012; 86: 2165–2175. https://doi.org/10.1128/JVI.06042-11 PMID: 22156533

39. Walton SM, Wyrsch P, Munks MW, Zimmermann A, Hengel H, Hill AB, et al. The dynamics of mouse cytomegalovirus-specific CD4 T cell responses during acute and latent infection. J Immunol. 2008; 181: 1128–1134. https://doi.org/10.4049/jimmunol.181.2.1128 PMID: 18606665

40. Zhang S, Springer LE, Rao H-Z, Trethewy RGE, Bishop LM, Hancock MH, et al. Hematopoietic cell-mediated dissemination of murine cytomegalovirus is regulated by NK cells and immune evasion. PLOS Pathog. 2021; 17: e1009255. https://doi.org/10.1371/journal.ppat.1009255 PMID: 33508041

41. Schlub TE, Sun JC, Walton SM, Robbins SH, Pinto AK, Munks MW, et al. Comparing the kinetics of NK cells, CD4, and CD8 T cells in murine cytomegalovirus infection. J Immunol. 2011; 187: 1385–1392. https://doi.org/10.4049/jimmunol.1100416 PMID: 21697462

42. Kim JH, Bryant H, Fiedler E, Cao T, Rayner JO. Real-time tracking of bioluminescent influenza A virus infection in mice. Sci Rep. 2022; 12: 3152. https://doi.org/10.1038/s41598-022-06667-w PMID: 35210462

43. Christoph S, Schlegel J, Alvarez-Calderon F, Kim Y-M, Brandao LN, DeRyckere D, et al. Bioluminescence imaging of leukemia cell lines in vitro and in mouse xenografts: effects of monoclonal and polyclonal cell populations on intensity and kinetics of photon emission. J Hematol OncolJ Hematol Oncol. 2013; 6: 10. https://doi.org/10.1186/1756-8722-6-10 PMID: 23343252

44. Byrne CM, Gantt S, Coombs D. Effects of spatiotemporal HSV-2 lesion dynamics and antiviral treatment on the risk of HIV-1 acquisition. PLOS Comput Biol. 2018; 14: e1006129. https://doi.org/10.1371/journal.pcbi.1006129 PMID: 29698393

45. Diekmann O, Heesterbeek JAP, Roberts MG. The construction of next-generation matrices for compartmental epidemic models. J R Soc Interface. 2010; 7: 873–885. https://doi.org/10.1098/rsif.2009.0386 PMID: 19892718

46. Cesario TC, Poland JD, Wulff H, Chin TD, Wenner HA. Six years experience with herpes simplex virus in a children's home. Am J Epidemiol. 1969; 90: 416–422. https://doi.org/10.1093/oxfordjournals.aje.a121087 PMID: 4311429

47. Schmitt DL, Johnson DW, Henderson FW. Herpes simplex type 1 infections in group day care. Pediatr Infect Dis J. 1991; 10: 729–734. https://doi.org/10.1097/00006454-199110000-00002 PMID: 1658720

48. Lanzieri TM, Dollard SC, Josephson CD, Schmid DS, Bialek SR. Breast milk-acquired cytomegalovirus infection and disease in very low birth weight and premature infants. Pediatrics. 2013; 131: e1937–e1945. https://doi.org/10.1542/peds.2013-0076 PMID: 23713111

49. Meier J, Lienicke U, Tschirch E, Krüger DH, Wauer RR, Prösch S. Human cytomegalovirus reactivation during lactation and mother-to-child transmission in preterm infants. J Clin Microbiol. 2005; 43: 1318–1324. https://doi.org/10.1128/JCM.43.3.1318-1324.2005 PMID: 15750102

50. Minamishima I, Ueda K, Minematsu T, Minamishima Y, Umemoto M, Take H, et al. Role of breast milk in acquisition of cytomegalovirus infection. Microbiol Immunol. 1994; 38: 549–552. https://doi.org/10.1111/j.1348-0421.1994.tb01821.x PMID: 7968688

51. Bryant P, Morley C, Garland S, Curtis N. Cytomegalovirus transmission from breast milk in premature babies: does it matter? Arch Dis Child—Fetal Neonatal Ed. 2002; 87: F75–F77. https://doi.org/10.1136/fn.87.2.f75 PMID: 12193509

52. Bardanzellu F, Fanos V, Reali A. Human Breast Milk-Acquired Cytomegalovirus Infection: Certainties, Doubts and Perspectives. Curr Pediatr Rev. 2019; 15: 30–41. https://doi.org/10.2174/1573396315666181126105812 PMID: 30474531

53. Zhang S, Caldeira-Dantas S, Smith CJ, Snyder CM. Persistent viral replication and the development of T cell responses after intranasal infection by MCMV. Med Microbiol Immunol (Berl). 2019; 208: 457–468. https://doi.org/10.1007/s00430-019-00589-7 PMID: 30848361

54. Nelson CS, Vera Cruz D, Su M, Xie G, Vandergrift N, Pass RF, et al. Intrahost Dynamics of Human Cytomegalovirus Variants Acquired by Seronegative Glycoprotein B Vaccinees. J Virol. 2019; 93: https://doi.org/10.1128/JVI.01695-18 PMID: 30518646

55. Griffiths PD, Baboonian C. A prospective study of primary cytomegalovirus infection during pregnancy: final report. Br J Obstet Gynaecol. 1984; 91: 307–315. https://doi.org/10.1111/j.1471-0528.1984.tb05915.x PMID: 6324849

56. Maloney JM, Sicherer SH. Passive immunization during pregnancy for congenital cytomegalovirus infection. Pediatrics. 2006; 118: S54–S54. https://doi.org/10.1542/peds.2006-0900KKKK

57. Lanzieri TM, Gastañaduy PA, Gambhir M, Plotkin SA. Review of mathematical models of vaccination for preventing congenital cytomegalovirus infection. J Infect Dis. 2020; 221: S86–S93. https://doi.org/10.1093/infdis/jiz402 PMID: 32134475

58. King AA, Nguyen D, Ionides EL. Statistical inference for partially observed Markov processes via the R package pomp. J Stat Softw. 2016; 69. https://doi.org/10.18637/jss.v069.i12

59. Padgett JMA, Ilie S. An adaptive tau-leaping method for stochastic simulations of reaction-diffusion systems. AIP Adv. 2016; 6: 035217. https://doi.org/10.1063/1.4944952